Solution of inverse medium scattering problems in electromagnetics by the adaptive Finite Element Method and Perfectly Matched Layer

Waldemar Rachowicz[1*] **and Witold Cecot**[2*]

[1]*Institute of Computer Science, Cracow University of Technology*
ul. Warszawska 24, 31-155 Cracow, Poland
e-mail: wrachowicz@pk.edu.pl

[2]*Institute for Computational Civil Engineering, Cracow University of Technology*
ul. Warszawska 24, 31-155 Cracow, Poland
e-mail: plcecot@cyf-kr.edu.pl

Abstract

The paper presents a study of solution of inverse medium scattering problems for time-harmonic electromagnetics in 3D. The solution is based on minimization of the misfit function between the observed scattered waves and trial solutions of direct problems for the sought approximate distribution of electric permittivity. The sources of illuminating waves and the observation points of the scattered fields are located in the vicinity of the scatterer. The simulations of the direct problems are performed with the adaptive Finite Element Method. Tests with real- and complex-valued distributions of electric permittivity, and with complete and incomplete measurement data are presented.

Keywords:inverse problems, electromagnetic field, finite element methods, adaptivity, optimization

1. Introduction

Inverse medium scattering problem in electromagnetics consists in evaluating the distribution of electromagnetic material parameters, (possibly) complex-valued electric permittivity $\hat{\epsilon}$ or magnetic permeability $\hat{\mu}$ of a material body, from the measurements of the scattered electromagnetic waves due to known illuminations. The procedure has many potential applications including medical tomography, localization of burried objects, detection of material defects *etc*. The advantage of the so-called microwave tomography would be its non-invasive character, the significant contrast of $\hat{\epsilon}$ for tissues with medical condition like a tumor, low cost and easy access. Obviously, we expect that the resolution of the method could not be as good as the resolution of the X-ray or Magnetic Resonance Imaging (MRI) techniques. Yet, the aforementioned advantages might make the method very useful for early detection of the decease.

Algoritms for solving inverse medium scattering problems in electromagnetics were investigated by Vögeler [1], Bao and Li [2], Hohage [3], Bulyshev *et al.* [4], Fhager *et al.* [5]., and other researchers.

2. Scattering problem

We consider scattering problem in time-harmonic electromagnetics. The electromagnetic field satisfies the time-harmonic Maxwell equations.

$$\begin{aligned} \boldsymbol{\nabla} \times \boldsymbol{E} &= -j\hat{\mu}\omega \boldsymbol{H}, \\ \boldsymbol{\nabla} \times \boldsymbol{H} &= j\hat{\epsilon}\omega \boldsymbol{E} + \boldsymbol{J}^{imp}, \end{aligned} \tag{2.1}$$

where $\boldsymbol{E}$ and $\boldsymbol{H}$ denote the electric and magnetic fields, $\boldsymbol{J}^{imp}$ is the impressed current, $j = \sqrt{-1}$ is the imaginary unit and ω is the circular frequency. Parameters $\hat{\epsilon}$ and $\hat{\mu}$ are the complex electric permittivity and magnetic permeability. In this work $\hat{\epsilon} = \epsilon - j\sigma/\omega$ and $\hat{\mu} = 1$, where ϵ and σ are the electric permittivity and conductivity (for simplicity, throughout this work we use the system of units in which the electric permittivity and magnetic permeability of the free space, $\epsilon_0 = \mu_0 = 1$). A common approach is to eliminate one of the fields, e.g. $\boldsymbol{H}$, and to use the electric field formulation which we state in Eq. 2.2.

In scattering problems we look for a perturbation of the prescribed incident electric field $\boldsymbol{E}^{in}$ caused by placing in the free space a non-homogeneous dielectric object, see Figure1.

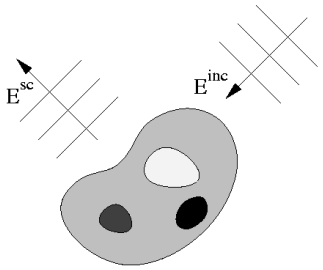

Figure 1: Scattering problem of electromagnetics

This perturbation is called the scattered field $\boldsymbol{E}^{sc}$. The total electric field $\boldsymbol{E}^{tot} = \boldsymbol{E}^{in} + \boldsymbol{E}^{sc}$, satisfies the reduced wave equation of electromagnetics:

$$\boldsymbol{\nabla} \times \hat{\mu}^{-1} \boldsymbol{\nabla} \times \boldsymbol{E}^{tot} - \omega^2 \hat{\epsilon}\, \boldsymbol{E}^{tot} = -j\omega \boldsymbol{J}^{imp}, \tag{2.2}$$

resulting from elimination of the magnetic field from Maxwell's equations (2.1). If we consider a non-magnetic material, $\hat{\mu} = 1$, which is the case for biological tissues, Eq. (2.2) results in the following formulation for $\boldsymbol{E}^{sc}$:

$$\boldsymbol{\nabla} \times \hat{\mu}^{-1} \boldsymbol{\nabla} \times \boldsymbol{E}^{sc} - \omega^2 \hat{\epsilon}\, \boldsymbol{E}^{sc} = -j\omega \boldsymbol{J}^{imp} + \omega^2 (\hat{\epsilon} - 1) \boldsymbol{E}^{in}. \tag{2.3}$$

* Acknowledgement. The work of W. Rachowicz and W. Cecot was supported by Polish Ministry of Higher Education, under grant N N519 405 234.

($\boldsymbol{E}^{in}$ satisfies the wave equation in the free space, i.e. with $\hat{\mu} = \hat{\epsilon} = 1$). We can look for the solution of Eq. (2.3) in a bounded domain Ω by assuming that the Dirichlet and Neumann traces of the scattered field, $\gamma_D(\boldsymbol{E}^{sc}) := \boldsymbol{E}^{sc} \times \boldsymbol{n}$, and $\gamma_N(\boldsymbol{E}^{sc}) := 1/k\boldsymbol{\nabla} \times \boldsymbol{E}^{sc} \times \boldsymbol{n}$, (where $k = \omega(\mu\epsilon)^{1/2}$ is the wavenumber) are related by the DtN-operator $\mathcal{G}$ of $\mathbb{R}^3 \setminus \Omega$

$$\frac{1}{k}\boldsymbol{\nabla} \times (\boldsymbol{E} - \boldsymbol{E}^{in}) \times \boldsymbol{n} = \mathcal{G}[(\boldsymbol{E} - \boldsymbol{E}^{in}) \times \boldsymbol{n}] \quad \text{on} \quad \Gamma, \tag{2.4}$$

which can be evaluated using the Boundary Element Method (BEM) [6], the Perfectly Matched Layer (PML) technique [7], Infinite Elements (IE) or Impedance Boundary Conditions (IBC) [8]. By multiplying the wave equation (2.3) by a test function $\boldsymbol{F}$, integrating it over domain Ω and integrating by parts the term with second derivatives we end up with the following variational formulation: find $\boldsymbol{E}^{sc}$ such that

$$a(\boldsymbol{E}^{sc}, \boldsymbol{F}) = l(\boldsymbol{F}), \quad \forall \boldsymbol{F}, \tag{2.5}$$

with $a(\cdot,\cdot)$ and $l(\cdot)$ denoting the following bilinear and linear forms:

$$\begin{aligned} a(\boldsymbol{E}^{sc}, \boldsymbol{F}) &= \int_\Omega (\boldsymbol{\nabla} \times \boldsymbol{E}^{sc} \cdot \boldsymbol{\nabla} \times \boldsymbol{F} - \omega^2 \hat{\epsilon} \boldsymbol{E}^{sc} \cdot \boldsymbol{F}) dx - \\ &\quad \frac{\omega}{Z_0} \int_\Gamma \mathcal{G}(\gamma_D \boldsymbol{E}^{sc}) \cdot \boldsymbol{F}\, dS, \\ l(\boldsymbol{F}) &= \int_\Omega [-j\omega \boldsymbol{J}^{imp} + \omega^2 (\hat{\epsilon} - 1)\boldsymbol{E}^{in}] \cdot \boldsymbol{F} dx \end{aligned} \tag{2.6}$$

where $Z_0 = (\mu_0/\epsilon_0)^{1/2}$ is the characteristic impedance of the free space. Alternatively, we may obtain the weak statement for the total field formulation (2.2) for which the functionals a and l are as follows:

$$\begin{aligned} a(\boldsymbol{E}^{tot}, \boldsymbol{F}) &= \int_\Omega (\boldsymbol{\nabla} \times \boldsymbol{E}^{tot} \cdot \boldsymbol{\nabla} \times \boldsymbol{F} - \omega^2 \hat{\epsilon} \boldsymbol{E}^{tot} \cdot \boldsymbol{F}) dx - \\ &\quad \frac{\omega}{Z_0} \int_\Gamma \mathcal{G}(\gamma_D \boldsymbol{E}^{tot}) \cdot \boldsymbol{F}\, dS, \\ l(\boldsymbol{F}) &= \frac{\omega}{Z_0} \int_\Gamma [\mathcal{G}(\gamma_D \boldsymbol{E}^{in}) + \gamma_N(\boldsymbol{E}^{in})] \cdot \boldsymbol{F}\, dS, \\ &\quad -j\omega \textstyle\int_\Omega \boldsymbol{J}^{imp} \cdot \boldsymbol{F} dx. \end{aligned} \tag{2.7}$$

The least expensive approximation of the DtN-operator can be defined by a local relation of traces of the scattered solution

$$\boldsymbol{n} \times (\boldsymbol{n} \times \boldsymbol{E}^{sc}) = Z_0 \boldsymbol{n} \times \frac{1}{j\mu\omega} \boldsymbol{\nabla} \times \boldsymbol{E}^{sc}, \tag{2.8}$$

it suffers, however, an irreducable modeling error unlike the IE or BEM techniques.

The PML technique has the advantage over the above methods that it can be used for a layered medium. It consists in replacing the true electric permittivity ϵ and magnetic permeability μ by the corresponding tensors $\boldsymbol{\epsilon}$ and $\boldsymbol{\mu}$ characterising orthotropic medium with damping properties in relatively thin layers surrounding the computational domain with compact sources. The solution rapidly decays in the layer and we can impose a homogeneous Dirichlet boundary condition on the external boundary of the layer. For rectangular, cylindrical and spherical layers the distribution of $\boldsymbol{\epsilon}$ and $\boldsymbol{\mu}$ can be designed in such a way that the exact solution of the scattering problem with PML is identical with the exact solution in the whole free space. The only problem is to approximate accurately enough the rapidly decaying waves in the PML. We can do this, for instance, by appropriate enrichment of the FE mesh. An example of a FEM mesh of order $p = 2$ with layers of elements of the order enriched to $p = 4$ for approximation of a decaying solution in PML is shown in Fig. 2.

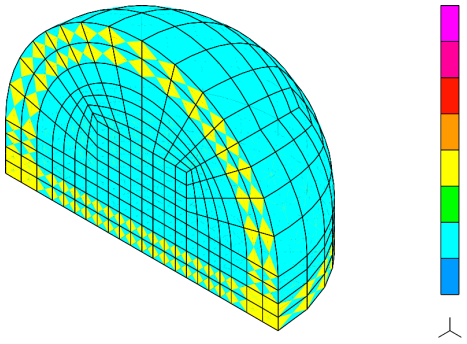

Figure 2: Finite element mesh of elements od order $p = 2$ with the enriched layers to approximate the solution in PML

The tensors of electric permittivity and magnetic permeability in PML take the following form:

$$\boldsymbol{\epsilon} = \epsilon \boldsymbol{\Lambda}, \quad \boldsymbol{\mu} = \mu \boldsymbol{\Lambda}, \tag{2.9}$$

where for cylindrical PML

$$\boldsymbol{\Lambda} = \frac{Z'}{R'}\frac{R}{r}\boldsymbol{e}_r \otimes \boldsymbol{e}_r + R'Z'\frac{r}{R}\boldsymbol{e}_\theta \otimes \boldsymbol{e}_\theta + \frac{R'}{X'}\boldsymbol{e}_z \otimes \boldsymbol{e}_z \tag{2.10}$$

while for the spherical PML

$$\boldsymbol{\Lambda} = \frac{1}{R'}\frac{R}{r}\boldsymbol{e}_r \otimes \boldsymbol{e}_r + R'\boldsymbol{e}_\theta \otimes \boldsymbol{e}_\theta + R'\boldsymbol{e}_\psi \otimes \boldsymbol{e}_\psi, \tag{2.11}$$

where $\boldsymbol{e}_r, \boldsymbol{e}_\theta, \boldsymbol{e}_z$ and $\boldsymbol{e}_r, \boldsymbol{e}_\theta, \boldsymbol{e}_\psi$ are the basis vectors of the cylindrical and spherical co-ordinates, respectively. In the above formulas $Z = Z(z)$, $R = R(r)$ are complex-valued functions of the cylindrical co-ordinates (z, r) or spherical coordinate r, respectively. They are designed to provide smooth decay of the waves in PML. These so-called "stretch functions" in this work are selected as

$$R(r) = \left[1 + jC\left(\frac{r - r_0}{\Delta r}\right)^3 / \lambda\right] r \tag{2.12}$$

where λ is the wavelength, r_0 is the internal radius of PML, Δr is its thickness, and $C = 2^6$. Outside PML $R(r) = r$. The definition of $Z(z)$ is analogous except that we must distinguish the upper and bottom PML of the cylinder.

The weak formulation for both, the scattered and total fields with PML is analogous to formulations discussed above though we neglect the presence of the DtN-operator $\mathcal{G}$.

3. Inverse medium scattering problem

The inverse medium scattering problem consists in reconstructing the distribution of material parameters characterizing the medium, in our case $\hat{\epsilon}(\boldsymbol{x})$, based on observation of the scattered waves due to some prescribed incident fields. We consider the location of both, the sources of the incident waves and the receivers in the vicinity of the scatterer. This is motivated by the desire to construct the method close to possible practical applications.

The set up of the inverse problem is as follows. We consider the sources of illuminating waves (transmitters) and observation points of the scattered field (receivers) as located at a finite and small distance from the scatterer. They are spread almost uniformly over a sphere of radius R containing the scatterer or over a half of this sphere. We consider M incident waves $\boldsymbol{E}^{in}_m$ which

come from radiating dipoles (modeling the transmitters) and N observation points $\boldsymbol{x}_n$.

The incident field radiated by a dipole takes form [9]:

$$\boldsymbol{E}^{in} = \frac{e^{-jkr}}{4\pi r}\left[\boldsymbol{q}\left(k^2 - \frac{jk}{r} - \frac{1}{r}\right) + \hat{\boldsymbol{r}}(\hat{\boldsymbol{r}}\cdot\boldsymbol{q})\left(-k^2 + \frac{3jk}{r} + \frac{3}{r^2}\right)\right] \tag{3.13}$$

where $\boldsymbol{q}$ is the moment of the dipole, $\boldsymbol{r}$ location of the point relative to the dipole, $r = |\boldsymbol{r}|$, and $\hat{\boldsymbol{r}} = \boldsymbol{r}/r$.

As an alternative way of generating illuminating waves we consider the following local distribution of the impressed current (in cylinrical co-ordinates):

$$\begin{cases} J_r^{imp} = -\left(\frac{r}{\epsilon}\right)^{\alpha}\left(1-\frac{r}{\epsilon}\right)^{\beta} a'(z), \\ J_z^{imp} = a(z)\left(\frac{r}{\epsilon}\right)^{\alpha-1}\left(1-\frac{r}{\epsilon}\right)^{\beta-1}[(\alpha+1)-(1+\alpha+\beta)\frac{r}{\epsilon}], \\ J_\phi^{imp} = 0, \end{cases} \tag{3.14}$$

where $\alpha = \beta = 3$ and $a(z) = [1-(z/\delta)^2]^3$. The support of $\boldsymbol{J}^{imp}$ is contained in a cylinder of radius δ and hight 2δ. The distribution is axisymmetric, solenoidal and smooth, C^1-continuous. We distribute these sources of waves analogously as pointwise dipoles, however they are located inside the computational domain. We use $\boldsymbol{J}^{imp}$ as a source of waves in the case the scatterer is located in the medium consisting of two half-spaces with different electric permittivities. For this case a closed formula for the field of the radiating dipole is not known so that illuminating waves must be found numerically. This can be easily done for the smooth $\boldsymbol{J}^{imp}$ as opposed to the pointwise dipole.

The scattered field at the observation point $\boldsymbol{y}$ outside computational domain Ω is evaluated based on the equivalence principle and using the following representation formula [10]:

$$\boldsymbol{p}(\boldsymbol{y},\boldsymbol{E}) \stackrel{not.}{=} \boldsymbol{E}^{sc}(\boldsymbol{y}) = \int_\Gamma [(\boldsymbol{E}\times\boldsymbol{n})\times\boldsymbol{\nabla}G - \boldsymbol{n}\times\boldsymbol{\nabla}\times\boldsymbol{E}G - (\boldsymbol{E}\cdot\boldsymbol{n})\boldsymbol{\nabla}G]dS \tag{3.15}$$

where $G = e^{-jkR}/(4\pi R)$ is Green's function for the scalar Helmholtz equation, $R = |\boldsymbol{y}|$, and Γ is any surface surrounding the scatterer (or point $\boldsymbol{y}$ in a homogeneous space). We note that $\boldsymbol{p}(\cdot,\boldsymbol{E})$ is a linear function.

At each observation point $\boldsymbol{x}_n$ we measure the scattered fields $\boldsymbol{E}^*_{mn}$ due to incident waves $\boldsymbol{E}^{in}_m$. We seek for the distribution $\hat{\epsilon}^*(\boldsymbol{x})$ by minimizing the discrepancy between the measured $\boldsymbol{E}^*_{mn}$ and the simulated $\boldsymbol{E}_{mn}$ corresponding to trial distributions $\hat{\epsilon}(\boldsymbol{x})$:

$$G = \sum_m \sum_n |\boldsymbol{E}_{mn} - \boldsymbol{E}^*_{mn}|^2 w_{mn} + \mathcal{M}(\hat{\epsilon}) \to \min \tag{3.16}$$

where w_{mn} are suitable weights and $\mathcal{M}$ is a regularizing functional. Trial distributions $\hat{\epsilon}(\boldsymbol{x})$ are approximated by a linear combination of trilinear FE shape functions $\phi_i, i = 1,\ldots,n$, on an auxiliary mesh covering a selected subdomain Ω_0, outside of which $\hat{\epsilon} = 1$:

$$\hat{\epsilon}(\boldsymbol{x}) = \begin{cases} \sum_{i=1}^{n} \phi_i(\boldsymbol{x})\hat{\epsilon}_i & \text{in } \Omega_0, \\ 1 & \text{in } \mathbb{R}^3 \setminus \Omega_0, \end{cases} \tag{3.17}$$

$\hat{\epsilon}_i \in \mathbb{C},\ i = 1,\ldots,n$, where $\Omega_0 \subset \Omega$ is an *a priori* known domain containing the scatterer.

The optimization is performed with the deterministic technique, the quasi-Newton Broyden-Fletcher-Goldfarb-Shanno (BFGS) method in the implementation of Zhu, Byrd and Nocedal [11]. It allows one to account for the natural constraints $Re(\hat{\epsilon}) \geq 1$ and $Im(\hat{\epsilon}) \leq 0$. We evaluate gradient of functional G using the method of adjoint problem (see for instance Petryk and Mróz [12]) to be discussed next.

4. The adjoint problem

We recall the idea to evaluate $\boldsymbol{\nabla}_\epsilon F(\hat{\epsilon})$ using the adjoint problem. Let us first state the way parameters $\hat{\epsilon}_i$ enter the problem in bilinear form a and linear functional l:

$$a(\boldsymbol{E},\boldsymbol{E}) = \int_\Omega [\mu^{-1}\boldsymbol{\nabla}\times\boldsymbol{E}\cdot\boldsymbol{\nabla}\times\boldsymbol{E} - \omega^2 \underbrace{(\sum_i \phi_i(\boldsymbol{x})\hat{\epsilon}_i)}_{\hat{\epsilon}(x)}\boldsymbol{E}\cdot\boldsymbol{F}]\,dx$$
$$l(F) = \omega^2 \int_\Omega [\underbrace{(\sum_i \phi_i(\boldsymbol{x})\hat{\epsilon}_i)}_{\hat{\epsilon}(x)} - 1]\boldsymbol{E}^{in}\cdot\boldsymbol{F}\,dx \tag{4.18}$$

For simplicity let us consider first the case of a real-valued weak formulation ($\sigma = 0, \hat{\epsilon}_i = \epsilon_i \in \mathbb{R}$, $\boldsymbol{E}$, $\boldsymbol{F}$ and $a(\boldsymbol{E},\boldsymbol{F}) - l(\boldsymbol{F})$ are real-valued). We consider an augmented real-valued functional

$$G = F(\boldsymbol{E}) + \underbrace{a(\boldsymbol{E},\boldsymbol{E}^a) - l(\boldsymbol{E}^a)}_{=0}, \tag{4.19}$$

where $\boldsymbol{E}^a$ plays the role of the Lagrangian multiplier and a test function. We investigate a variation of G due to an infinitesimal perturbation $\delta\boldsymbol{\epsilon}$ of parameters $\boldsymbol{\epsilon} = \{\epsilon_1,\ldots,\epsilon_n\}^T$.

$$\delta G = \underbrace{\boldsymbol{\nabla}_E F\ \delta\boldsymbol{E} + a(\delta\boldsymbol{E},\boldsymbol{E}^a)}_{=0} + \underbrace{a(\boldsymbol{E},\delta\boldsymbol{E}^a) - l(\delta\boldsymbol{E}^a)}_{=0} + (\boldsymbol{\nabla}_\epsilon a\ \delta\boldsymbol{\epsilon})(\boldsymbol{E},\boldsymbol{E}^a) - (\boldsymbol{\nabla}_\epsilon l\ \delta\boldsymbol{\epsilon})(\boldsymbol{E}^a) \tag{4.20}$$

where, following (3.17), we have

$$\{(\boldsymbol{\nabla}_\epsilon a)(\boldsymbol{E},\boldsymbol{E}^a)\}_i = -\omega^2\int_\Omega \phi_i(\boldsymbol{x})\boldsymbol{E}\cdot\boldsymbol{E}^a\,dx,$$
$$\{(\boldsymbol{\nabla}_\epsilon l)(\boldsymbol{E}^a)\}_i = \omega^2\int_\Omega \phi_i(\boldsymbol{x})\boldsymbol{E}^{in}\cdot\boldsymbol{E}^a\,dx \tag{4.21}$$

(for total field formulation (2.7) $\boldsymbol{\nabla}_\epsilon l = 0$) and the two of indicated terms vanish due to the weak formulation for $\boldsymbol{E}$ and due to the condition to be stated in (4.22). Namely, we define the solution of the *adjoint problem* as a solution of the following weak statement: find $\boldsymbol{E}^a$ such that

$$a(\delta\boldsymbol{E},\boldsymbol{E}^a) + \boldsymbol{\nabla}_E F\ \delta\boldsymbol{E} = 0,\ \ \forall\ \delta\boldsymbol{E}. \tag{4.22}$$

Therefore, with this choice of $\boldsymbol{E}^a$, we find that the gradient of G can be expressed as:

$$\boldsymbol{\nabla}_\epsilon G = \boldsymbol{\nabla}_\epsilon a(\boldsymbol{E},\boldsymbol{E}^a) - \boldsymbol{\nabla}_\epsilon l(\boldsymbol{E}^a). \tag{4.23}$$

Now we remove the restriction that the form $a(\boldsymbol{E},\boldsymbol{E}^a) - l(\boldsymbol{E}^a)$ is real-valued. We note that the weak formulation of electromagnetics is in a way redundant. The following three conditions are equivalent

$$\begin{aligned} & a(\boldsymbol{E},\boldsymbol{F}) - l(\boldsymbol{F}) = 0,\ \forall \text{ complex-valued } \boldsymbol{F} \\ \Leftrightarrow\ & a(\boldsymbol{E},\boldsymbol{F}) - l(\boldsymbol{F}) = 0,\ \forall \text{ real-valued } \boldsymbol{F} \\ \Leftrightarrow\ & Re\{a(\boldsymbol{E},\boldsymbol{F}) - l(\boldsymbol{F})\} = 0,\ \forall \text{ complex-valued } \boldsymbol{F} \end{aligned} \tag{4.24}$$

This lets us choose the third option of the above to define the real-valued augmented functional with $\boldsymbol{F} = \boldsymbol{E}^a$ as follows:

$$G = F(\hat{\epsilon}) + Re\{a(\boldsymbol{E}, \boldsymbol{E}^a) - l(\boldsymbol{E}^a)\}, \tag{4.25}$$

and evaluation of $\boldsymbol{\nabla}_\epsilon G$ must be modified accordingly. It should be emphasized that solution of the adjoint problem adds no significant computational burden because the forward and adjoint formulations share the same stiffness matrix which is triangulated only once.

5. Finite Element discretization

Solution of direct problems in Ω are approximated using the FEM with hexahedral edge elements. We use the FE code with a capability of hp-refinements. That is, we can selectively subdivide elements reducing their size h and nonuniformly change their spectral orders p [8]. Both operations can be anisotropic. The code is equipped with an algorithm for automatic hp-adaptivity. The unbouned computational domain can be truncated using approximation of the DtN-operator of the external domain with the Infinite Elements, Boundary Element Method, Absorbing Boundary Conditions, or Perfectly Matched Layer technique. The last approach is favoured in this work as, in prospect, it will allow us to model a part of the human body adjacent to the rest of the body.

The systems of linear equations resulting from the FEM discretization are solverd with the direct solver MUMPS [13] on 8 processors.

6. Numerical examples

Our motivation of solving inverse medium scattering problems is the possibility of reconstructing the distribution of the complex electric permittivity $\hat{\epsilon}(\boldsymbol{x})$ from the measurements of scattered fields. Such distribution would provide a three-dimensional image of the scatterer. A frequently used procedure of investigating inverse problem solution algorithms is to use numeriacally simulated measurements. That is we obtain the scattered fields at measurement points for the prescribed distribution of $\hat{\epsilon}^*(\boldsymbol{x})$ and we perturb them to mimic the measurement errors. This is also our way of running tests.

The antennas are distributed over a sphere of radius R. Their distribution is close to uniform and it is obtained as follows. We subdivide the sphere into 6 identical quadrilateral patches bounded by 6 planes $x_i = \pm x_j, i, j = 1, 2, 3, i \neq j$. For each patch we consider 2 families of k intermediate planes between the separating planes, rotated by the angle of $(i-1)\pi/(2k),\ i = 1, \ldots, k+1$. Intersections of planes of both families and the sphere define locations of transmitters/receivers. The number of these points is $(k+1)^3 - (k-1)^3 = 26, 56, \ldots$ for $k = 2, 3, \ldots$. We assume that each transmitter is a source of waves of two mutually orthogonal polarizations tangential to the sphere. In actual tests it was sufficient to use $k = 2$, i.e. 26 receivers/transmitters and 52 illuminating waves.

We solve the test problems with real- and complex-valued distributions of $\hat{\epsilon}$. We also consider the tests with the measurement data obtained for points spread over the entire surface surrounding the scatterer, and the tests based on measurements obtained on a half of the sphere. We refer to these two situations as the complete and incomplete data cases. The measurement perturbation is of the form $\boldsymbol{E}_{mn} \rightarrow \boldsymbol{E}_{mn}(1 + \text{rand} \cdot a)$ with rand$\in [-1, 1]$ being a uniformly distributed random number, and $a = 0.1$ is the amplitude of the noise.

We use the waves of the free spece wavelength $\lambda = 2$ (only in the first example $\lambda = 1$). In other words the unit of length is $\lambda/2$. In all tests optimization required less than 100 solutions of direct problems.

6.1. Two Gaussian hills

We consider the following distribution of real-valued electric permittivity:

$$\epsilon(\boldsymbol{x}) = \begin{cases} 1 + b(\boldsymbol{x}) \cdot x_2^2 \cdot e^{-(x_1^2+x_2^2+x_3^2)/a^2}, & \text{if } \boldsymbol{x} \in (-1,+1)^3, \\ 1, & \text{otherwise,} \end{cases} \tag{6.26}$$

where

$$b(\boldsymbol{x}) = 12.5[(1-x_1^2)(1-x_2^2)(1-x_3^2)]^2, \quad a = 2/3 \tag{6.27}$$

Similar distribution was investigated by Bao and Li [2]. Figure 3a presents the finite element mesh. We solved the problem in a ball of radius $r = 2$. It is truncated by the PML of the thickness $\Delta r = 0.7$. The distribution of ϵ is reconstructed in $\Omega_0 = [-1, 1]^3$. The incident waves are generated by 26 dipoles located on a sphere of radius $R = 3$ where we also put the 26 measurement points. The exact and reconstructed distributions of $\epsilon(\boldsymbol{x})$ are shown in Fig. 3b-e. Accuracy of the recovered ϵ was 7% in the L^2-norm. We used the scattered field formulation.

6.2. Kidney-like scatterer

In this test we consider real-valued ϵ and incomplete scattering data. The distribution of electric permittivity is defined as follows:

$$\begin{aligned} &\epsilon(\boldsymbol{x}) = \begin{cases} 1 + [27/4(-r^3 + r^2)]^2, & \text{if } \boldsymbol{x} \in (-1,+1)^3 \\ 1, & \text{otherwise} \end{cases} \\ &r^2 = (y_1/a)^2 + (y_2/b)^2 \\ &\begin{cases} y_1 = \rho \arcsin[x_1/(1.5\rho)], \\ y_2 = \rho - 1 \end{cases} \\ &\rho = [(x_3 + 0.005)^2 + (x_1/1.5)^2]^{1/2} \end{aligned} \tag{6.28}$$

where $f = r^3 - r^2$ is a Hermite polynomial such that $f(0) = f'(0) = f(1) = 0, f'(1) = 1$. The function above is extended to 3D by rotational symmetry w.r.t. x_3-axis, i.e. by substitution $x_1 \rightarrow \sqrt{x_1^2 + x_2^2}$. The contours of $\epsilon(\boldsymbol{x})$ resemble the shape of a kidney. The scatterer is placed in the computational domain Ω in the form of an upper half of a ball of radius $r = 3$ extended by a cylindrical part at the bottom. It is truncated by the PML of the thickness $\Delta r = 0.7$. The incident waves are radiated by the dipoles located on the upper hemisphere of radius $r = 2.5$, i.e. inside Ω, and we use the scattered field formulation. The scattered field at the measurement points is evaluted via formula (3.15) with Γ being a boundary of the domain bounded by the spheres of radii 2 and 3 and the z-plane. The exact and reconstructed distributions of $\epsilon(\boldsymbol{x})$ are shown in Fig. 4. We reached the accuracy of 11%.

6.3. Kidney-like scatterer with a tumor

We consider the distribution of complex-valued electric permittivity $\hat{\epsilon}(\boldsymbol{x})$. The real part is defined as in (6.28) while the imaginary part, $Im(\hat{\epsilon}) = -\frac{1}{2} Re(\hat{\epsilon})$. In addition, we modify these distributions by local "bumps"-tumors that we define as follows:

$$\epsilon(\boldsymbol{x}) \longrightarrow \epsilon(\boldsymbol{x}) \cdot [1 + c(1 - d^2/r^2)], \tag{6.29}$$

where $d = |\boldsymbol{x} - \boldsymbol{t}|$ and $\boldsymbol{t}$ is the central point of the tumor, r is its radius. Parameter $c > 0$ defines the contrast of the perturbation. Function $\epsilon(\boldsymbol{x})$ is modified only if $|\boldsymbol{x} - \boldsymbol{t}| < r$. We set $\boldsymbol{t} = (0.0,\ 0.5,\ 0.5)$, $r = 0.5$ and $c = 2$ for the real part and $\boldsymbol{t} = (0.0,\ 0.5,\ 0.25)$, $r = 0.5$ and $c = 1$ for the imaginary part. In this example we use the incomplete data. The transmitters and receivers are located on the upper hemisphere of radius

2.5 inside Ω. This was motivated by the desire to mimic the possible conditions of medical examination (for instance of a brest). The transmitters are modeled by the localized impressed currents as defined in (3.14), with z-axis corresponding to one of two directions of polarizations. We use the total field formulation. The finite element mesh is identical as in the previous example. The exact and recovered electric permittivity is presented in Fig. 5 and 6. We observe satisfactory resolution of the "tumors" in the reconstructed image.

6.4. Brest-like scatterer with a tumor

In our last example we consider scattering on an object located in the medium consisting of two half-spaces of different electric properties, separated by the horizontal plane. In the upper half-space $\hat{\epsilon} = (1, 0)$ while in the bottom one $\hat{\epsilon} = (2, -1)$. The scatterer occupies the upper half-ball of radius $r = 1$ and it is adjacent with its basis to the plane separating the two half-spaces. The distribution of $\hat{\epsilon}$ is specified as follows:

$$\begin{aligned} &Re(\hat{\epsilon}) = f^2(r), \;\; r = \sqrt{x_1^2 + x_2^2 + x_3^2} \;\text{ for }\; r < 1, \\ &Im(\hat{\epsilon}) = -\tfrac{1}{2} Re(\hat{\epsilon}), \end{aligned} \tag{6.30}$$

where f is the Hermite polynomial as in (6.28). The contours of ϵ are half-circles. In addition, as in the previous example, we add local perturbations, bumps–tumors (6.29), that we define by the following parametrs: for the real part $\boldsymbol{t} = (0.0,\ 0.7,\ 0.7)$, $r = 0.5$ and $c = 2$, and for the imaginary part $\boldsymbol{t} = (0.0,\ 0.435,\ 0.9)$, $r = 0.5$ and $c = 1$.

Both, the sources of incident waves and observation points are located on a northern hemisphere of radius 2.5 inside the computational domain. We use the local impressed currents as defined in (3.14) as the transmitters. In fact they were designed just for this kind of problems as we do not know the closed formula for the field of a radiating dipole in a two half-spaces medium. The evaluation of the scattered field was performed as in the previous test. We present the exact and reconstructed distributions in Fig. 7 and 8. As before satisfactory resolution of of the local perturbations of $\hat{\epsilon}$ is observed. The accuracy of 11% was reached. This example reflects a procedure of examination of a female brest with medical condition, with the two half-spaces modeling the human body and the free space.

7. Conclusions

We presented a method for solving inverse medium scattering problems in electromagnetics. It is based on minimization of the misfit function between the measured scattered waves and the simulated scattered fields corresponding to trial distributions of electric permittivity. The reconstructed distribution of complex electric permittivity can be considered as a 3D image of the scattering object which justifies calling the method microwave tomography. The wavelength of the illuminating waves is comparable to the size of the scatterer. In the case of illuminating biological tissues the method is harmless as it causes no ionisation. Another advantage of the method is high contrast of tissues affected by medical condition.

We used the deterministic BFGS optimization algorithm to solve the minimization problem. The gradient of the goal function is established using the adjoint problem technique. The inverse solution algorithm was tested for real- and complex-valued distributions of electric permittivity, and for complete and incomplete scattering data. Small local perturbations of $\epsilon(\boldsymbol{x})$ were successfully detected. The method returned satisfactory results in numerical tests resembling examination of a part of a human body with a medical condition like a tumor.

Finally, we mention that error control for direct problems is possible by means of adaptive capability of the finite element code. This issue was discussed in [14].

References

[1] Vogeler, M., Reconstruction of the three-dimensional refractive index in electromagnetic scattering by using a propagation–backpropagation method. *Inverse Problems* 19, pp. 739-753, 2003.

[2] Bao, G., Li, P., Numerical solution of an inverse medium scattering problem for Maxwells Equations at fixed frequency. *J. Comp. Physics*, 228, pp. 4638-4648, 2009.

[3] Hohage, Th., Fast numerical solution of the electromagnetic medium scattering problem and applications to the inverse problem. *J. Comp. Physics*, 214, pp. 224-228, 2006.

[4] Bulyshev, A.E., Souvorov, A.E., Semenov, S.Y., Posukh, V.G., and Sizov, Y.E., Three-dimensional vector microwave tomography: theory and computational experiments. *Inverse Problems*, 20, pp. 1239-1259, 2004.

[5] Fhager, A., Hashemzedeh, P., and Persson, M., Reconstruction quality and spectral content of electromagnetic time-domain inversion algorithm *IEEE Trans. Biomedical Engineering*, 8, 2006.

[6] Buffa, A., Hiptmair, R., Galerkin Boundary Element Methods for Electromagnetic scattering, in ÂĺComputational Methods in Wave Propagation,ÂĺM. Ainsworth et al. eds. Lecture Notes in Computational Science and Engrg., 31, pp. 83-124, Springer-Verlag 2003.

[7] Berenger, J.-P., A perfectly matched layer for the absorption of electromagnetic waves. *J. Comput. Phys.*, 114, pp. 185-200, 1994.

[8] Demkowicz, L., Kurtz, J., Pardo, D., Paszyński, M., Rachowicz, W., and Zdunek, A., *Computing with hp-Adaptive Finite Elements. vol.2: Frontiers: Three Dimensional Elliptic and Maxwell Problems with Applications* Chapman & Hall/CRC, Taylor and Francis Group, Boca Raton, FL 33487-2742, USA, 2008.

[9] Landau, L.D., Lifshitz, E. M. *The Classical Theory of Fields*, Addison-Wesley, Reading, Ma, 1971.

[10] Harrington, R.F., *Time-Harmonic Electromagnetic Fields*, McGrow-Hill, New York, 1961.

[11] Byrd, R. H., Lu, P., Nocedal, J., and Zhu, C., A limited memory algorithm for bound constrained optimization, *SIAM J. Scientific Computing*, 16, pp. 1190-1208, 1995.

[12] Petryk, H. and Mroz, Z., Time derivatives of integrals and functionals defined on varying volume and surface domains. *Arch. Mech.*, 38, pp. 694-724, 1986.

[13] Amestoy, P.R., Duff, I.S., and LÂt'Excellent, J.-Y., Multifrontal parallel distributed symmetric and unsymmetric solvers *Comput. Meth. Appl. Mech. Engrg.* 184, pp. 501-520, 2000.

[14] Rachowicz, W., , and Zdunek, A., Application of the FEM with Adaptivity for electromagnetic inverse medium scattering problems. *Comput. Meth. Appl. Mech. Engrg.* in press, 2011.

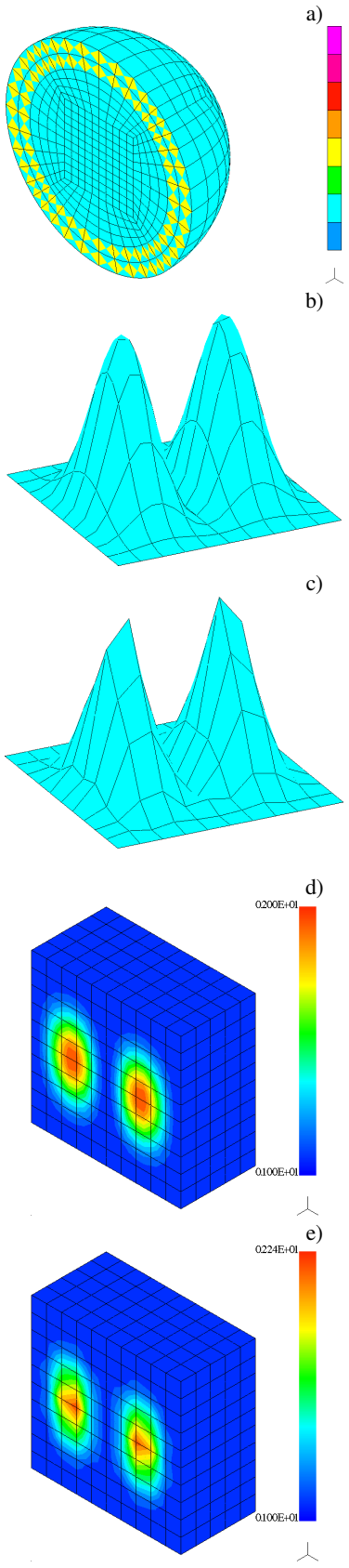

Figure 3: Two Gaussian hills scatterer. a) FE mesh, b), d) exact, and c), e) reconstructed real-valued electric permittivity $\epsilon(\boldsymbol{x})$

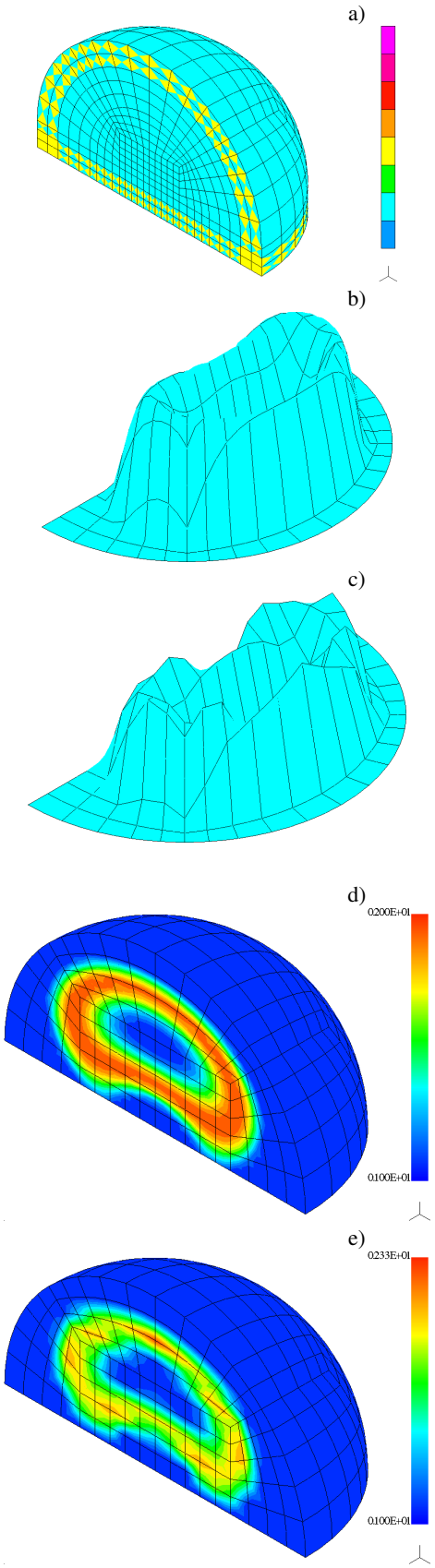

Figure 4: Kidney-like scatterer. a) FE mesh, b), d) exact, and c), e) reconstructed real-valued electric permittivity $\hat{\epsilon}(\boldsymbol{x})$

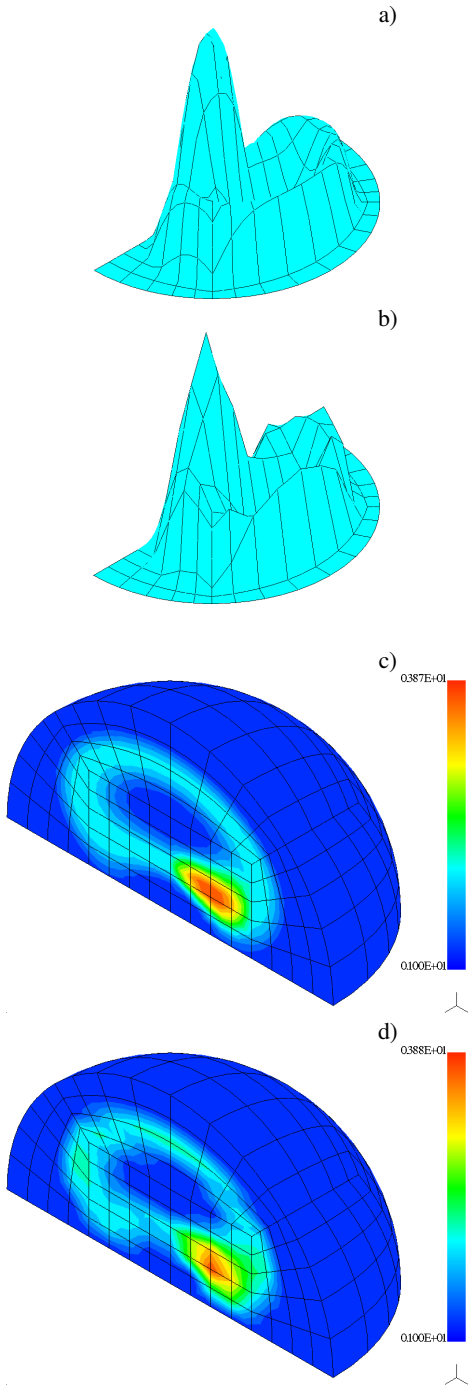

Figure 5: Kidney-like scatterer with tumors. a), c) exact, and b), d) reconstructed real part of complex electric permittivity $\hat{\epsilon}(\boldsymbol{x})$

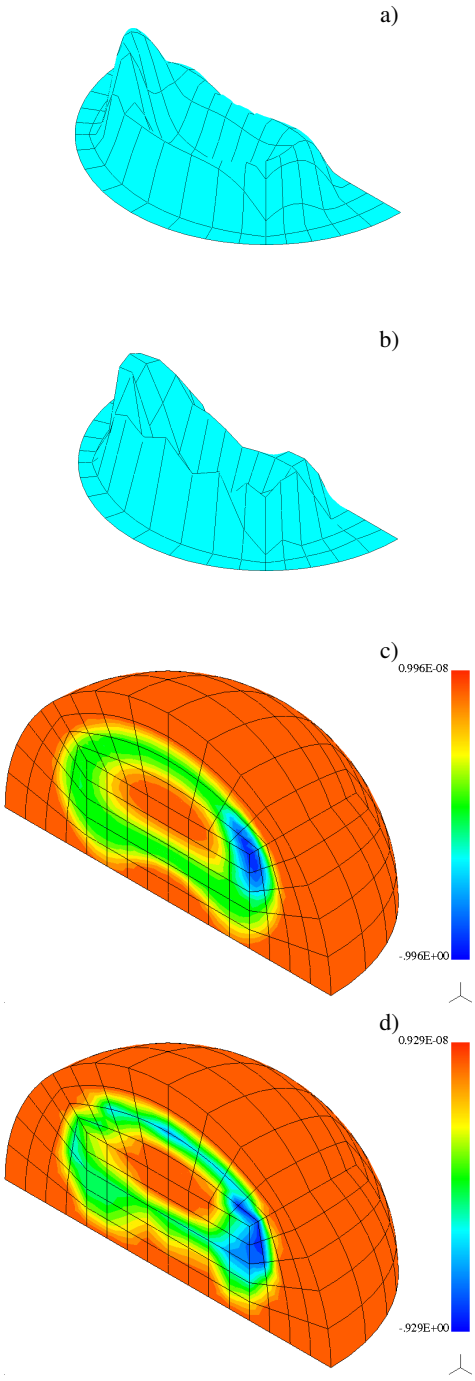

Figure 6: Kidney-like scatterer with tumors. a), c) exact, and b), d) reconstructed imaginary part of complex electric permittivity $\hat{\epsilon}(\boldsymbol{x})$

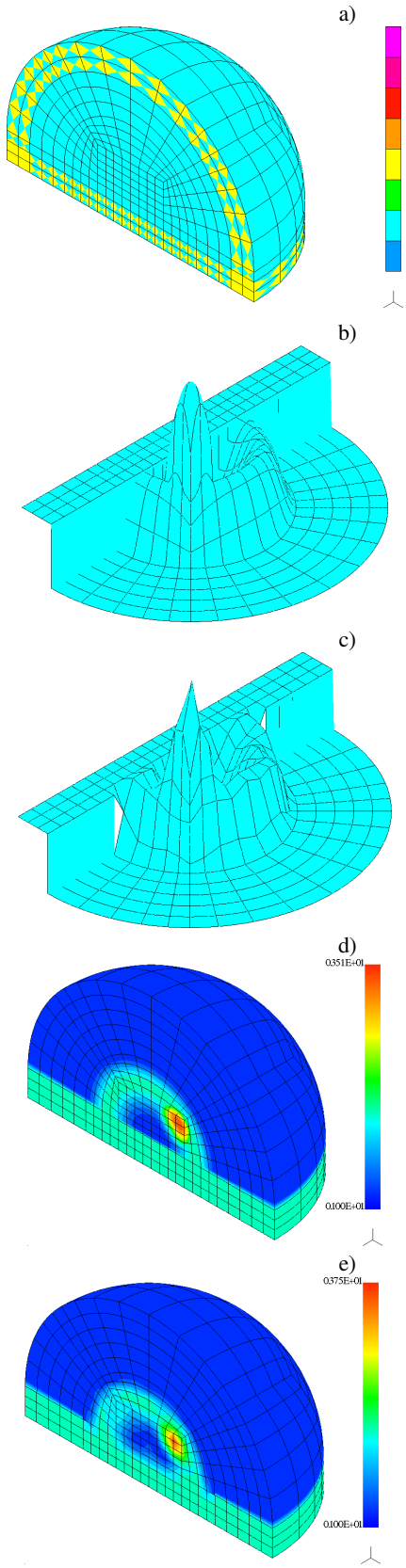

Figure 7: Scatterer with tumors in two half-spaces. a) FE mesh, b), d) exact, and c), e) reconstructed real part of complex electric permittivity $\hat{\epsilon}(\boldsymbol{x})$

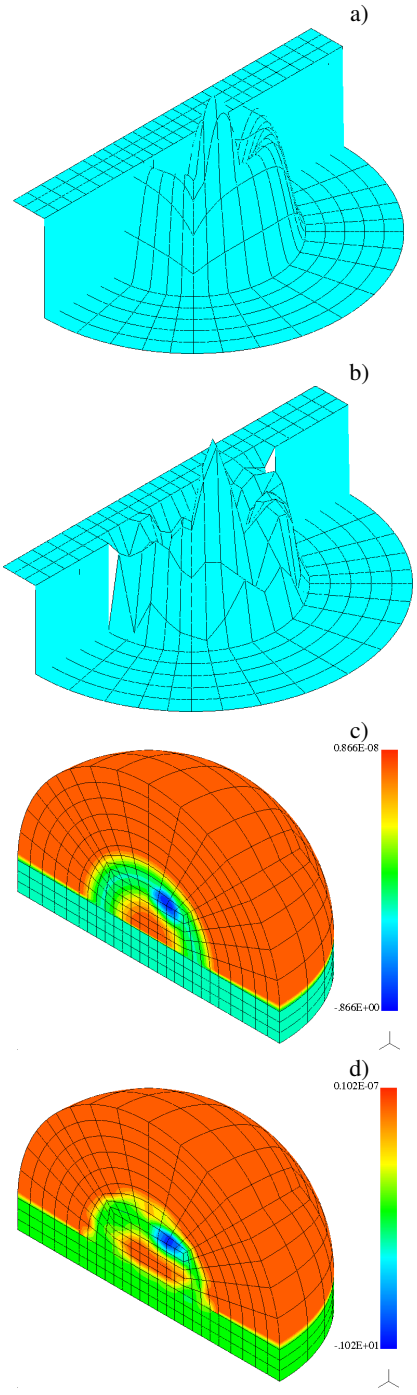

Figure 8: Scatterer with tumors in two half-spaces. a), c) exact, and b), d) reconstructed imaginary part of complex electric permittivity $\hat{\epsilon}(\boldsymbol{x})$